PNAS RESEARCH ARTICLE | NEUROSCIENCE OPEN ACCESS

Dopamine induces fear extinction by activating the reward-responding amygdala neurons

Xiangyu Zhang[a,b,1], Katelyn Flick[a,b,1], Marianna Rizzo[a,b,c], Michele Pignatelli[a,b,d], and Susumu Tonegawa[a,b,d,2]

Contributed by Susumu Tonegawa; received January 17, 2025; accepted March 25, 2025; reviewed by Joshua P. Johansen and Rebecca Shansky

The extinction of conditioned fear responses is crucial for adaptive behavior, and its impairment is a hallmark of anxiety disorders such as posttraumatic stress disorder. Fear extinction takes place when animals form a new memory that suppresses the original fear memory. In the case of context-dependent fear memory, the new memory is formed within the reward-responding posterior subset of basolateral amygdala (BLA) that is genetically marked by *Ppp1r1b*$^+$ neurons. These memory engram cells suppress the activity of the original fear-responding *Rspo2*$^+$ engram cells present in the anterior BLA, hence fear extinction. However, the neurological nature of the teaching signal that instructs the formation of fear extinction memory in the *Ppp1r1b*$^+$ neurons is unknown. Here, we demonstrate that ventral tegmental area (VTA) dopaminergic signaling drives fear extinction in distinct BLA neuronal populations. We show that BLA fear and extinction neuronal populations receive topographically divergent inputs from VTA dopaminergic neurons via differentially expressed dopamine receptors. Fiber photometry recordings of dopaminergic activity in the BLA reveal that dopamine (DA) activity is time-locked to freezing cessation in BLA fear extinction neurons, but not BLA fear neurons. Furthermore, this dopaminergic activity in BLA fear extinction neurons correlates with extinction learning. Finally, using projection-specific optogenetic manipulation, we find that activation of the VTA DA projections to BLA reward and fear neurons accelerated or impaired fear extinction, respectively. Together, this work demonstrates that dopaminergic activity bidirectionally controls fear extinction by distinct patterns of activity at BLA fear and extinction neurons.

fear extinction | dopamine | amygdala | reward | valence

Significance

The ability to extinguish fearful associations that are no longer relevant is crucial for survival. Understanding the neural circuits and neuromodulators that regulate fear extinction is necessary to improve treatment for many fear-related mental health disorders, like posttraumatic stress disorder (PTSD). New extinction memory is formed and stored in the basolateral amygdala (BLA). However, it has been unknown how the extinction learning is initiated in the BLA. Here, through a combination of in vivo dopamine recordings and functional manipulations, we show that dopamine acts differentially on distinct BLA subpopulations to control fear extinction learning.

The ability to extinguish fear associations is critical for maintaining a balance between negative and positive valances, and its impairment is detrimental to mental health (1, 2). Fear extinction is a form of new learning that allows for the adaptive control of fear behaviors and is commonly studied using simple Pavlovian conditioning tasks (3). The basolateral amygdala (BLA) is a key brain structure for fear extinction, with anatomically, genetically, and functionally distinct populations of neurons that control fear conditioning versus fear extinction (4–6). The BLA fear neurons, primarily located in the anterior BLA (aBLA), are genetically accessible by the *Rspo2* marker, while BLA extinction neurons, primarily located in the posterior BLA (pBLA), are genetically accessible by the *Ppp1r1b* marker (4, 7, 8). aBLA *Rspo*$^+$ neurons encode negative valence and drive aversive behaviors whereas pBLA *Ppp1r1b*$^+$ neurons encode positive valence and drive appetitive behaviors (8). During fear extinction, the new memory is formed and stored in the BLA Ppp1r1b+ neuronal population (4).

For extinction learning to occur, the absence of the aversive stimuli must be detected and relayed to brain structures mediating the formation of extinction memory, including the BLA *Ppp1r1b*$^+$ neuronal population. The omission of the expected aversive stimuli signals a better than expected outcome, which may generate a learning signal that drives the switch from fear to fear extinction circuitry in the BLA (9–11). The ventral tegmental area (VTA) dopamine system has a well-established role in encoding unpredicted outcomes and directing learning throughout the brain (12, 13). During fear extinction, a subpopulation of VTA dopaminergic neurons responds early to the omission of footshocks and this activity is necessary for extinction learning and retrieval (14–16). Recent work has identified a dopaminergic switch for fear to safety transition based on VTA to nucleus accumbens circuit and a VTA to prefrontal cortex circuit opposing the transition (14). Nevertheless, the target of VTA dopamine activity that is capable of initiating extinction learning is still unknown.

While evidence for the role of dopamine (DA) signaling in the amygdala comes from measurements of increased dopamine in the BLA in response to appetitive and aversive events (17–20), the functional role of the VTA to BLA pathway has received little attention (21). Recent work suggests that VTA projections to the BLA are active in response to

Author affiliations: [a]The Picower Institute for Learning and Memory, Department of Biology, Massachusetts Institute of Technology, Cambridge, MA 02139; [b]The Picower Institute for Learning and Memory, Department of Brain and Cognitive Sciences, Massachusetts Institute of Technology, Cambridge, MA 02139; [c]Dipartimento di Medicina e Chirurgia, Laboratorio di Neuroanatomia, Universitá di Parma, Parma 43125, Italy; and [d]HHMI at Massachusetts Institute of Technology, Cambridge, MA 02139

Author contributions: X.Z., K.F., and S.T. designed research; X.Z. and K.F. performed research; X.Z., K.F., M.R., and M.P. analyzed data; and X.Z., K.F., M.P., and S.T. wrote the paper.

Reviewers: J.P.J., RIKEN Noshinkei Kagaku Kenkyu Center; and R.S., Northeastern University.

The authors declare no competing interest.

[1]X.Z. and K.F. contributed equally to this work.

[2]To whom correspondence may be addressed. Email: tonegawa@mit.edu.

This article contains supporting information online at https://www.pnas.org/lookup/suppl/doi:10.1073/pnas.2501331122/-/DCSupplemental.

Published April 28, 2025.

appetitive and aversive stimuli, and during contextual fear memory extinction (22, 23). We should emphasize that in this study we examined the role of VTA projections to aversive stimuli-responding *Rspo2*$^+$ BLA neurons and appetitive stimuli-responding *Ppp1r1b*$^+$ BLA neurons in the context of fear and fear extinction memory. Here, we hypothesize that the omission of expected footshocks increases VTA dopaminergic activity at BLA *Ppp1r1b*$^+$ reward neurons and that this activity is necessary to initiate fear extinction (9–11). To test this hypothesis, we used anatomical tracing, fiber photometry recordings of DA activity, projection-specific optogenetic manipulations, and dopamine receptor manipulations in behaving mice to examine the role of dopamine on BLA neuronal populations during fear extinction.

Results

Differential VTA Dopamine Neurons Projections to BLA *Rspo2*$^+$ and *Ppp1r1b*$^+$ Neurons. To characterize the anatomical connection from VTA to BLA, we performed bidirectional circuit mapping using viral anterograde and monosynaptic retrograde tracing. To determine the density of VTA DA projections to the BLA, we injected a Cre-dependent virus expressing ChR2-EYFP into the VTA of DAT-IRES-Cre (dopamine transporter-Cre) mice (Fig. 1 *A* and *B*) and measured the axonal fluorescence in the lateral amygdala (LA), aBLA, and pBLA. Fluorescence intensity measurements revealed that pBLA receives stronger innervation from VTA dopamine neurons than aBLA, whereas LA receives only a very weak innervation (Fig. 1*C*).

Growing evidence supports the spatial organization of VTA dopaminergic subpopulations depending on their projection target and role in behavior (8, 24–26). Thus, we wondered whether BLA *Rspo2*$^+$ and *Ppp1r1b*$^+$ neurons received projections from different VTA subpopulations. To examine the distribution in the VTA of DA projections to BLA *Rspo2*$^+$ and *Ppp1r1b*$^+$ neurons, we used cell-type-specific monosynaptic rabies tracing. An AAV helper virus, AAV1-synP-FLEX-sTpEpB, was injected into the aBLA of *Rspo2*-Cre mice or pBLA of *Ppp1r1b*-Cre-mice and incubated for 3 wk before the injection of G-deleted rabies mCherry virus (27, 28). Dopaminergic cells in the VTA were identified by labeling with an antibody against TH (Tyrosine Hydroxylase) (Fig. 1 *D*–*G*). We found in the VTA a sparse population of retrogradely labeled TH$^+$ and TH$^-$ neurons projecting to BLA *Rspo2*$^+$ and *Ppp1r1b*$^+$neurons. TH$^+$ neurons projecting to BLA *Rspo2*$^+$ were primarily distributed in anterior and lateral left and right VTAs (average number of TH$^+$ cells n = 56 and of TH$^-$ cells n = 37 for n = 4 mice, Fig. 1*H*). In contrast, TH$^+$ neurons projecting to BLA *Ppp1r1b*$^+$ cells were mainly located in the medial posterior left and right VTAs (average number of TH$^+$ cells n = 34 and of TH$^-$ cells n = 7 for n = 3 mice, Fig. 1*H*). These results suggest that BLA *Rspo2*$^+$ and *Ppp1r1b*$^+$ neurons receive topographically divergent inputs from the VTA dopamine neurons.

Differential Expression of Dopamine Receptors in the BLA. The action of dopamine depends on postsynaptic dopamine receptors. The two classes of dopamine receptors, D1-class and D2-class, have opposing effects on neuronal activity via their second

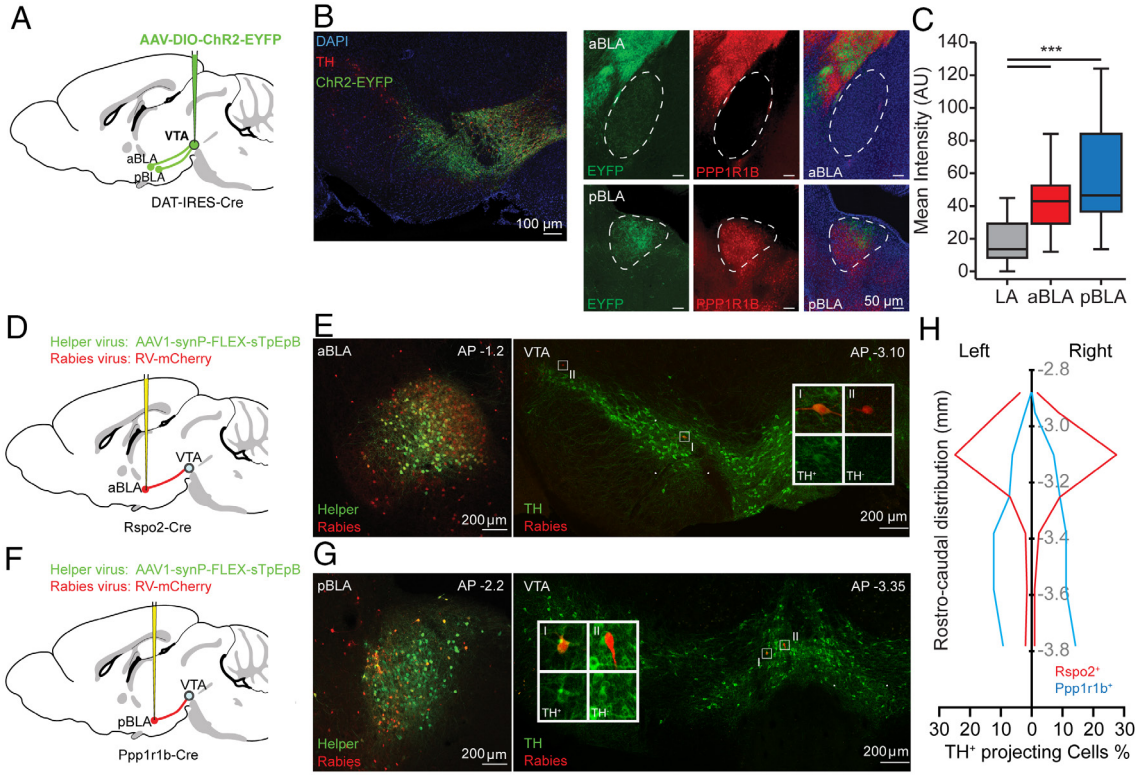

Fig. 1. Anterograde and retrograde tracing of VTA dopaminergic neurons to BLA. (*A*) Schematic of AAV9-DIO-ChR2-EYFP injection into VTA of DAT-IRES-Cre mice. (*B*) *Left*, representative image of ChR2-EYFP expression in the VTA, TH in red. *Right*, confocal images of anterograde EYFP-expressing fibers (green, *Left Top* and *Bottom*) through the medial–lateral axis of the BLA (red, *Middle-Top* Ppp1rb1$^-$ and *Middle-Bottom* Ppp1rb1$^+$ subregions; overlap on *Right Top-Bottom* panels, blue DAPI). (*C*) Quantification of mean pixel intensity in the LA, aBLA, and pBLA in arbitrary units (N = 3 replicate mice, n = 18 sections per region; One-way ANOVA, ***$P < 0.001$). (*D*) Schematic of helper and rabies virus injection into aBLA of Rspo2-Cre mice. (*E*) Representative confocal images of rabies-mediated retrograde tracing from BLA *Rspo2*$^+$ neurons to VTA dopaminergic neurons (*Inset*: I = TH$^+$ and II = TH$^-$ neurons projecting to *Rspo2*$^+$ neurons). (*F*) Schematic of helper and rabies virus injection into pBLA of Ppp1rb1-Cre mice. (*G*) Representative confocal images of rabies-mediated retrograde tracing from pBLA *Ppp1r1b*$^+$ neurons to VTA dopaminergic neurons (*Inset*: I = TH$^+$ and II = TH$^-$ neurons projecting to *Ppp1r1b*$^+$ neurons). (*H*) Bilateral rostro-caudal distribution of VTA dopaminergic cells projecting to *Rspo2*$^+$ (green, n = 208 cells) or *Ppp1r1b*$^+$ (red, n = 101 cells) neurons ($\chi^2 < 0.0001$, Rspo2-Cre mice N = 4, Ppp1r1b-Cre mice: N = 3, injections in the right hemisphere).

messenger pathways. D1-class receptors, which include D1 and D5, generally increase neuronal activity via cAMP production by adenyl cyclase. D2-class receptors, which include D2, D3, and D4, decrease neuronal activity by inhibiting adenyl cyclase in the postsynaptic cell (29).

Although the distribution of dopamine receptors in the amygdala has been well examined, no study to date has differentiated between aBLA and pBLA or the genetically identified subpopulations. To characterize the dopamine-receptor expression in BLA, we first performed double single-molecule fluorescent in situ hybridization (smFISH) targeting D1 and D2 receptor in anterior and pBLA along the rostrocaudal axis (Fig. 2*A*). Then, to simultaneously detect D1 and D2 receptors in Rspo2 and Ppp1r1b expressing neurons, we performed multiplexed smFISH (Fig. 2*B*). We observed stronger expression of D1 receptors in the BLA *Ppp1r1b*$^+$ neuronal population as compared to *Rspo2*$^+$ neurons (Fig. 2*C*). Consistent with previous results, D2 receptor expression was visible in the CeA and ITC, but not in BLA *Rspo2*$^+$ or *Ppp1r1b*$^+$ neurons (Fig. 2 *A* and *B*) (30, 31). These experiments provide a complete description of the overlap between D1 and D2 dopamine receptor expression in the BLA and the *Rspo2*$^+$ and *Ppp1r1b*$^+$neuronal populations.

Dopaminergic Activity in BLA *Ppp1r1b*$^+$ Neuronal Population in Response to Fear Extinction Learning. The BLA plays a critical role in contextual fear conditioning and extinction (32–34), and in particular, the BLA *Ppp1r1b*$^+$ neuronal population is the site of contextual fear extinction memory formation and storage (4). Thus, to understand the role of DA in fear extinction, we combined a contextual fear extinction protocol with fiber photometry of DA signal. On day 1, mice received contextual fear conditioning (CFC) in a behavioral chamber where the context served as the conditioned stimulus (CS) and three rounds of footshocks served as unconditioned stimulus (US). On day 2, mice were returned to the conditioning chamber for 45 min in the absence of footshocks for contextual fear extinction training. On day 3, the mice were tested for 10 min extinction memory retrieval in the conditioning chamber (Fig. 3 *A*–*C*).

To gain insight into real-time dopaminergic activity in the BLA *Rspo2*$^+$ and *Ppp1r1b*$^+$ neurons and its relationship with the freezing state of the animals during fear memory extinction, we performed fiber photometry recordings of a genetically encodable fluorescent dopamine indicator, GRABda, in BLA *Rspo2*$^+$ or *Ppp1r1b*$^+$ neurons (35). We targeted expression to BLA *Rspo2*$^+$ or *Ppp1r1b*$^+$ neurons by injection of a Cre-dependent viral vector carrying

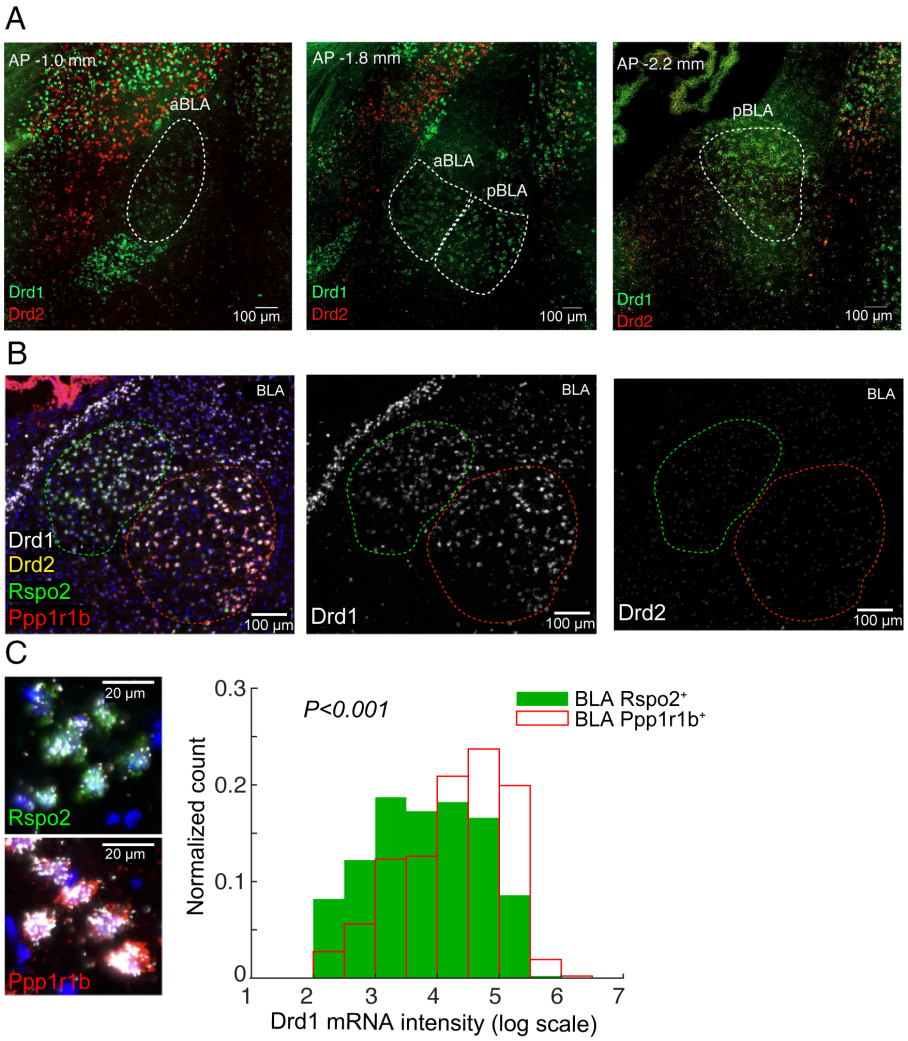

Fig. 2. Quantification of D1 and D2 dopamine receptor expression in the BLA. (*A*) Double smFISH of *Drd1* (green) and *Drd2* (red) in BLA along the AP axis. (*B*) Fourplex smFISH of *Drd1* (white) and *Drd2* (yellow), *Rspo2* (green, and green dotted line) and *Ppp1rb1* (red, and red dotted line) in BLA. (*C*) *Left*: high magnification images showing colocalization of neurons containing both *Drd1* and *Rspo2* or *Ppp1r1b* mRNA in BLA. *Right*: normalized count of double positive cells (*Rspo2-Drd1* green, and *Ppp1r1b-Drd1* red) plotted as a function of the *Drd1* mRNA fluorescence intensity. *Rspo2* cells: n = 272; *Ppp1r1b* cells: n = 325. Unpaired *t* test, *P* = 2.5*10^6.

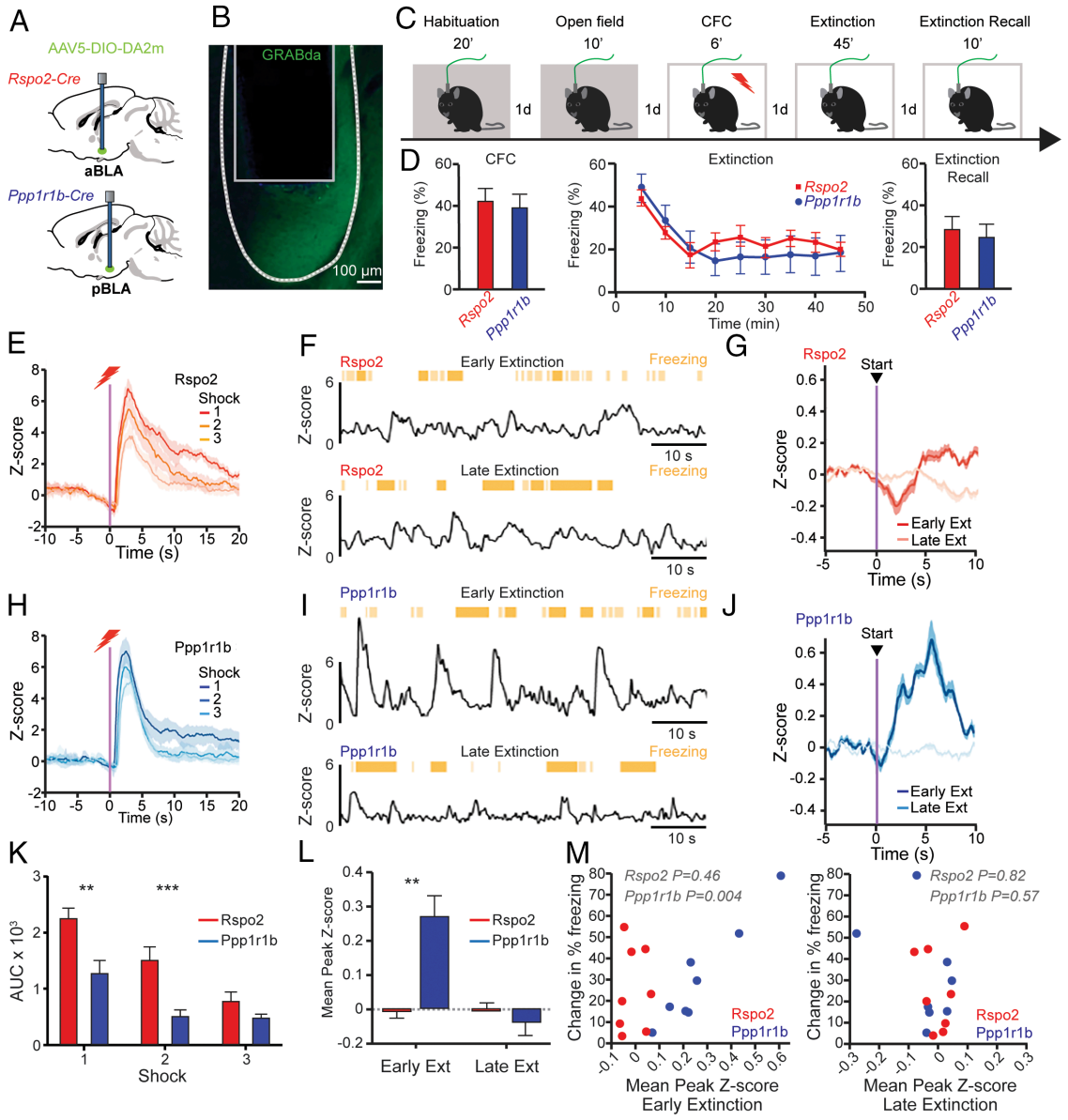

Fig. 3. Dopamine activity in BLA *Ppp1r1b*$^+$ neurons is correlated with extinction learning. (*A*) Schematic of the fiber photometry implant. (*B*) Confocal image displaying aBLA of Rspo2-Cre mouse expressing the dopamine sensor GRABda (green) and fiber optic track (squared box). (*C*) Schematic of the experimental setup: 35 d after surgery, mice were habituated to the photometry setup and connected to the patch cord for 20 min in the home cage, and underwent an open field test, contextual fear conditioning, extinction, and extinction recall. (*D*) Group average freezing levels after shock (*Left*), during extinction (*Middle*), and extinction recall during first 3 min (*Right*). (*E*) Group average dopamine activity to shock onset for three shock trials for *Rspo2*$^+$ neurons. (*F*) Example traces of photometry signals (reported as z-score) during early (*Top*) and late (*Bottom*) extinction in *Rspo2*$^+$ neurons. Yellow boxes above the traces indicate freezing bouts (0.5 s > light yellow < 2 s; dark yellow >= 2 s). (*G*) Dopamine activity aligned to transition from freezing (>0.5 s) to movement (>3 s) during early and late extinction in *Rspo2*$^+$ neurons. (*H*) Group average dopamine activity to shock onset for three shock trials for *Ppp1r1b*$^+$ neurons. (*I*) Example traces of photometry signals (reported as z-score) during early (*Top*) and late (*Bottom*) extinction in Ppp1r1b-Cre mice. Yellow boxes above the traces indicate freezing bouts. (*J*) Dopamine activity aligned to transition from freezing (>0.5 s) to movement (>3 s) during early and late extinction in *Ppp1r1b*$^+$ neurons. (*K*) Postpeak area under the curve for each shock. *Rspo2*$^+$ neurons display a response stronger than *Ppp1r1b*$^+$ neurons (unpaired *t* test, $^{**}P < 0.01$). (*L*) Quantification of the peak z-score observed in the 3 s after freezing cessation in *Rspo2*$^+$ and*Ppp1r1b*$^+$ neurons in early and late extinction (unpaired *t* test, $^{**}P < 0.01$, $^{***}P < 0.001$). *Ppp1r1b*$^+$ neurons display a response stronger than *Rspo2*$^+$ neurons. (*M*) *Left*: correlation between the average peak z-score observed in the 3 s after freezing cessation in *Rspo2*$^+$ and *Ppp1r1b*$^+$ neurons during early extinction and the change in percent freezing from early to late extinction (Spearman's correlation: Rspo2, R = 0.31, *P* = 0.46; Ppp1r1b, R = 0.88, *P* = 0.0039). *Right*: correlation between the average peak z-score observed in the 3 s after freezing cessation in *Rspo2*$^+$ and *Ppp1r1b*$^+$ neurons during late extinction and the change in percent freezing from early to late extinction (Spearman's correlation: Rspo2, R = 0.11, *P* = 0.82; Ppp1r1b, R = −0.24, *P* = 0.57). For all panels: n = 8 Rspo2-Cre, n = 8, Ppp1r1b-Cre. $^{**}P < 0.01$; $^{***}P < 0.001$. Error bars or shaded regions indicate SEM.

GRABda (AAV5-DIO-DA4.4) to the aBLA of Rspo2-Cre mice or the pBLA of Ppp1r1b-Cre mice and recorded GRABda emission using a DORIC single site photometry setup (Fig. 3 *A* and *B*).

Recent data show that VTA dopaminergic neuronal activity strongly correlates with learning during early extinction, suggesting that in the release of dopamine in the BLA could provide a learning signal that initiates fear extinction (36). Throughout the 45-min contextual fear extinction session, freezing dropped significantly during the first 15 min and stabilized thereafter (Fig. 3*D*). Thus, for analysis of dopaminergic activity, we refer to the first 15 min and last 15 min of extinction training as early and late extinction, respectively.

To study the relationship between dopaminergic activity in BLA and extinction learning, we aligned photometry traces to freezing cessation and filtered for movement bouts that lasted longer than 3 s. Both BLA *Rspo2*$^+$ and *Ppp1r1b*$^+$ neurons displayed a strong

increase in dopamine activity during shock although BLA *Rspo2*$^+$ neurons produced a larger response (Fig. 3 *E*, *H*, and *K*). Strikingly, we found that *Ppp1r1b*$^+$ neurons exhibited significantly increased dopamine activity after freezing cessation during early extinction when shock omission was unexpected (Fig. 3 *F*, *G*, *I*, and *J*). In contrast, during late extinction, dopamine activity no longer correlated with freezing cessation, suggesting that the observed increase in dopamine activity was specific to extinction learning and not an artifact of movement (Fig. 3*L*).

If dopamine release in BLA *Ppp1r1b*$^+$ extinction neurons drives extinction learning, then the increase in dopamine signal to freezing cessation during early extinction should be larger in animals that exhibit stronger extinction learning. To test this, we took advantage of the variability in the extinction learning of individual mice and asked whether they were correlated with dopamine activity at freezing cessation in early extinction. The extinction learning rate was measured as the percent change in freezing from the first to last 5-min bin of extinction. This revealed a significant correlation between the peak dopamine signal during early extinction and the change in freezing in *Ppp1r1b*-Cre mice, but not *Rspo2*-Cre (Spearman's correlation, Ppp1r1b, R = 0.88, $P = 0.0039$; Rspo2, R = 0.31, $P = 0.46$ Fig. 3*M*). We also examined the correlation between the change in freezing and peak dopamine signal during late extinction and did not find a significant relationship in either population of neurons, though notably dopamine activity in the BLA is significantly decreased in late extinction (Spearman's correlation: Rspo2, R = 0.11, $P = 0.82$; Ppp1r1b, R = –0.24, $P = 0.57$; Fig. 3*M*).

VTA Dopamine Activity in BLA Controls Fear Extinction. Our finding that dopaminergic activity specifically in *Ppp1r1b*$^+$ neurons was correlated with extinction learning suggests that dopamine activity has different behavioral functions in BLA *Rspo2*$^+$ and *Ppp1r1b*$^+$ populations during fear extinction. Our anatomical tracing experiments confirm that the primary dopaminergic input to BLA neurons originates from the VTA. Therefore, to investigate the contribution of VTA-BLA projections in fear extinction, we optogenetically manipulated VTA dopaminergic terminals in the aBLA (corresponding to *Rspo2*$^+$ neurons) or pBLA (corresponding to *Ppp1r1b*$^+$ neurons) during fear extinction training (Fig. 4*A*). We injected a Cre-dependent AAV carrying ChR2 (channelrhodopsin-2) or NpHR3.0 (halorhodopsin) into the VTA of DAT-IRES-Cre mice and implanted optical fibers targeting the aBLA or pBLA (Fig. 4*B*). Starting 5 min after the onset of extinction training, a 3-min blue or green laser pulse was delivered repeatedly at 2-min intervals. On day 3, mice were returned to the conditioning chamber for 5 min to test for extinction memory retrieval (Fig. 4*A*).

We first asked whether the observed dopamine activity is necessary for fear extinction. Optogenetic inhibition of DA terminals in pBLA dramatically impaired both extinction learning and retrieval (Fig. 4 *E* and *F*). In contrast, inhibition of DA terminals in aBLA did not affect freezing behavior during extinction or retrieval (Fig. 4 *I* and *J*), suggesting that dopamine activity in aBLA is not necessary for fear recall.

If VTA dopaminergic neuron activity is not only necessary for fear extinction, but also a driver of fear extinction learning, then increasing VTA DA activity should be sufficient to alter the course of extinction learning. Indeed, activation of VTA DA terminals in pBLA accelerated extinction learning promotingsubsequent fear extinction retrieval (Fig. 4 *C* and *D*). Unexpectedly, activation of VTA DA terminals in aBLA did not alter changes in freezing behavior during early extinction but caused an increase in freezing in late extinction, resembling fear relapse. This fear relapse resulted in impaired extinction retrieval the next day (Fig. 4 *G* and *H*).

These results demonstrate that VTA dopaminergic activity can bidirectionally control fear extinction learning through its projection to pBLA *Ppp1r1b*$^+$ neurons and suggest a role for VTA-aBLA *Rspo2*$^+$ neurons in mediating fear behavior.

Manipulation of D1 Dopamine Receptor in the BLA. To determine how dopamine modulates distinct BLA populations during behavior, we applied a viral approach to selectively manipulate the D1 receptor expression in aBLA *Rspo2*+ neurons or pBLA *Ppp1r1b*+ neurons (Fig. 5 *A* and *B*). D1 receptors were overexpressed by injecting AAV5-Ef1a-DIO-Drd1-EYFP into the aBLA of Rspo2-Cre mice or the pBLA of Ppp1r1b-Cre mice (Fig. 5 *C* and *D*). To knock down D1 receptors, we constructed a Cre-dependent AAV expressing a short hairpin RNA (shRNA) against the mouse D1 receptor (Drd1), AAV5-CAG-DIO-GFP-mDRD1a-shRNAmir (Fig. 5 *E* and *F*). A scrambled shRNA sequence was used as a negative control. Overexpression and knockdown (KD) efficiency in vivo were assessed by smFISH quantification (Fig. 5 *C*–*F*). Both groups underwent the same 3-d contextual fear extinction protocol as described before (Fig. 5*B*). All groups exhibited identical learning curves during fear conditioning (Fig. 5 *G* and *I*). In BLA *Ppp1r1b*+ neurons, overexpression of Drd1 impaired fear recall and promoted extinction training (Fig. 5*G*), whereas KD of Drd1 impaired fear extinction and retrieval (Fig. 5*H*). In BLA *Rspo2*+ neurons, KD of D1 receptors induced a lower freezing level during both fear recall and extinction retrieval (Fig. 5*J*), but Drd1 overexpression did not affect fear extinction behavior (Fig. 5*I*).

These results suggest that Drd1-mediated dopamine transmission accelerates extinction via *Ppp1r1b*+ neurons (4).

Discussion

In this study, we explored the dopaminergic modulation of the BLA with a focus on contextual fear extinction and BLA cell subpopulations. We previously showed that the shift from fear to safety in the fear extinction process is mediated by *Ppp1r1b*$^+$ reward-responding neurons and their inhibition of the original *Rspo2*$^+$ fear memory neurons (4). Here, we reveal that distinct populations of dopaminergic neurons in the VTA project to aBLA *Rspo2*$^+$ fear neurons and pBLA *Ppp1r1b*$^+$reward neurons. During fear extinction, the dopaminergic activity in *Ppp1r1b*$^+$ neurons aligns with freezing cessation and correlates with fear extinction learning. We showed that fear extinction requires VTA dopaminergic activity in the pBLA *Ppp1r1b*$^+$ neurons by using optogenetic inhibition of VTA terminals and cell-type-specific KD of D1 receptors in these neurons. In addition, optogenetic activation of VTA dopaminergic terminals directly in BLA *Ppp1r1b*$^+$ neurons accelerates extinction learning. Furthermore, we have previously shown a mutual antagonism between *Rspo2*$^+$ fear neurons and *Ppp1r1b*$^+$reward neurons, which is characterized by reciprocal GABAergic inhibition (8). As a consequence, a strong neuronal activation of *Ppp1r1b*$^+$neurons may lead to the suppression of *Rspo2*$^+$ neurons, switching the valence of the context from negative to positive (7). These findings suggest that dopaminergic activity in the BLA *Ppp1r1b*$^+$ reward neurons induces extinction learning (see schematic model in Fig. 6).

During fear extinction, the discrepancy between the expectation, i.e., CS-paired shocks, and the actual outcome, i.e., absence of aversive US, has been thought to generate a *teaching signal* for fear extinction learning (11, 14, 37). Our data suggest that this signal is encoded by VTA dopaminergic neuron activity, which responds to shock omission and is necessary for fear extinction learning

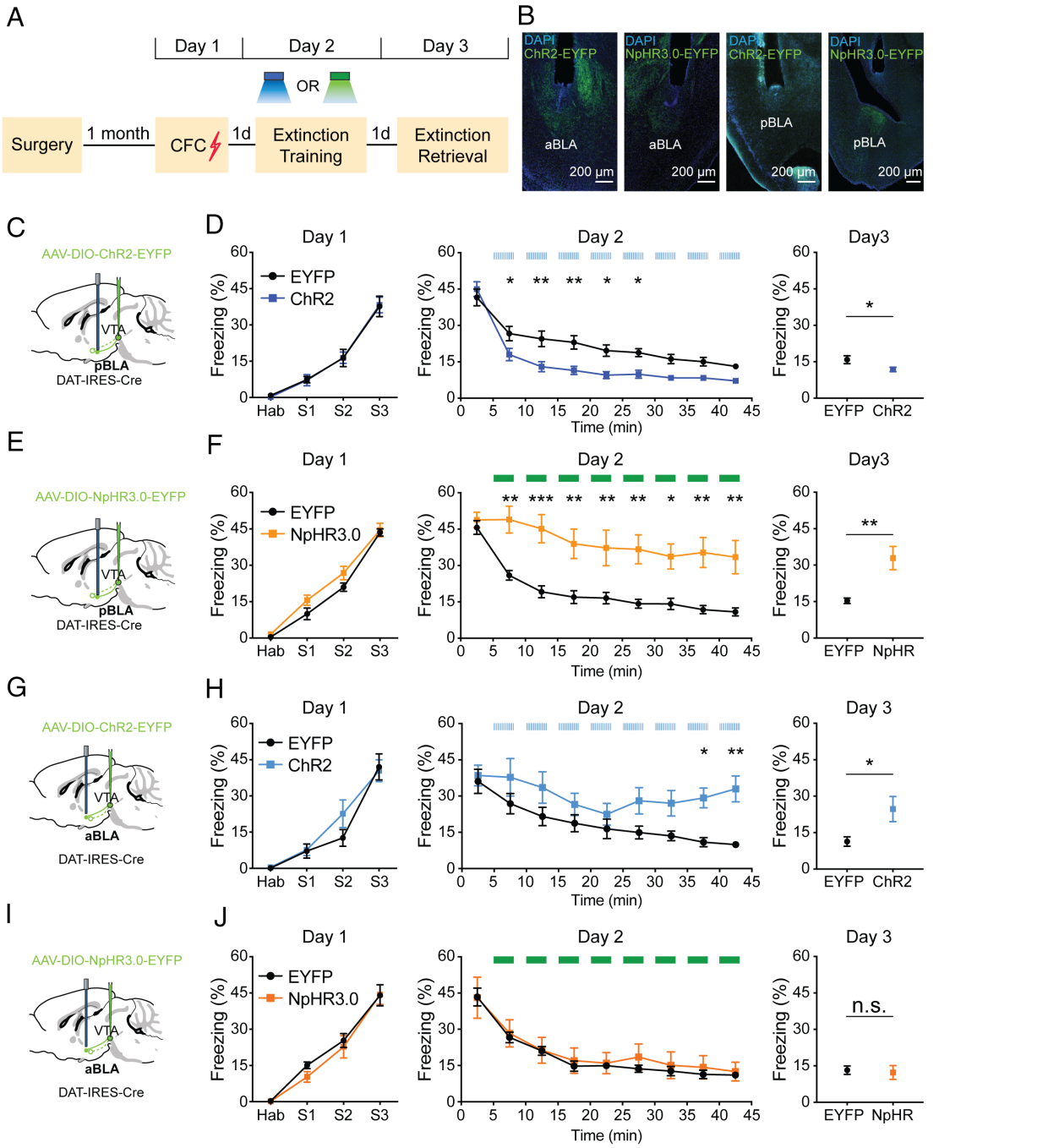

Fig. 4. Bidirectional control of fear extinction by optogenetic manipulation of VTA Dopaminergic projection to pBLA or aBLA. (*A*) Experimental protocol of optogenetic manipulation during fear extinction training. (*B*) Confocal images showing fiber optic placement and ChR2-YFP$^+$ or NpHR3.0-EYFP$^+$ DA axons in anterior and pBLA in relation to schematics (*C*, *E*, *G*, and *I*), respectively. (*C*) Schematic of AAV-DIO-ChR2-EYFP injection into VTA and optical fiber implant targeting pBLA of DAT-IRES-Cre mice. (*D*) Optogenetic activation of VTA dopaminergic projections to pBLA facilitated fear extinction learning and fear extinction memory. EYFP group n = 9; ChR2 group n = 10. Day1 and Day 2: Two-way RM ANOVA; Day 3: Unpaired *t* test. (*E*) Schematic of AAV-DIO-NpHR3.0-EYFP injection into VTA and optical fiber implant targeting pBLA of DAT-IRES-Cre mice. (*F*) Optogenetic inhibition of VTA dopaminergic projections to pBLA impaired fear extinction learning and fear extinction memory. EYFP group n = 11; NpHR group n = 10. Day 1 and Day 2: Two-way RM ANOVA; Day 3: Unpaired *t* test. (*G*) Schematic of AAV-DIO-ChR2-EYFP injection into VTA and optical fiber implant targeting aBLA of DAT-IRES-Cre mice. (*H*) Optogenetic activation of VTA dopaminergic projections to aBLA suppressed fear extinction learning and fear extinction memory. EYFP group n = 8; ChR2 group n = 8. Day 1 and Day 2: Two-way RM ANOVA; Day 3: Unpaired *t* test. (*I*) Schematic of AAV-DIO-NpHR3.0-EYFP injection into VTA and optical fiber implant targeting aBLA of DAT-IRES-Cre mice. (*J*) Optogenetic inhibition of VTA dopaminergic projections to aBLA did not affect fear extinction behavior. EYFP group n = 9; NpHR group n = 8. Day 1 and Day 2: Two-way RM ANOVA; Day 3: Unpaired *t* test. Data are presented as mean ± SEM. **P* < 0.05, ***P* <0.01, ****P* <0.001, *****P* <0.0001.

(14–16). Previous studies did not establish a target of VTA dopaminergic neurons capable of initiating fear extinction learning (14, 36). Our study directly examined dopaminergic modulation onto genetically tagged *Rspo2*$^+$ BLA fear and *Ppp1r1b*$^+$ extinction neurons and identified the latter as the target of VTA dopaminergic activity as a teaching signal for extinction learning.

VTA Topology of Appetitive and Aversive Encoding. We identified an anterior to posterior gradient of VTA dopamineergic neurons projecting to *Rspo2*$^+$ neurons and *Ppp1r1b*$^+$ neurons, respectively. In the intermediate VTA, there was also a medial to lateral gradient of *Ppp1r1b*$^+$ projectors and *Rspo2*$^+$ projectors, respectively. Overall VTA projections to distinct BLA subpopulations are

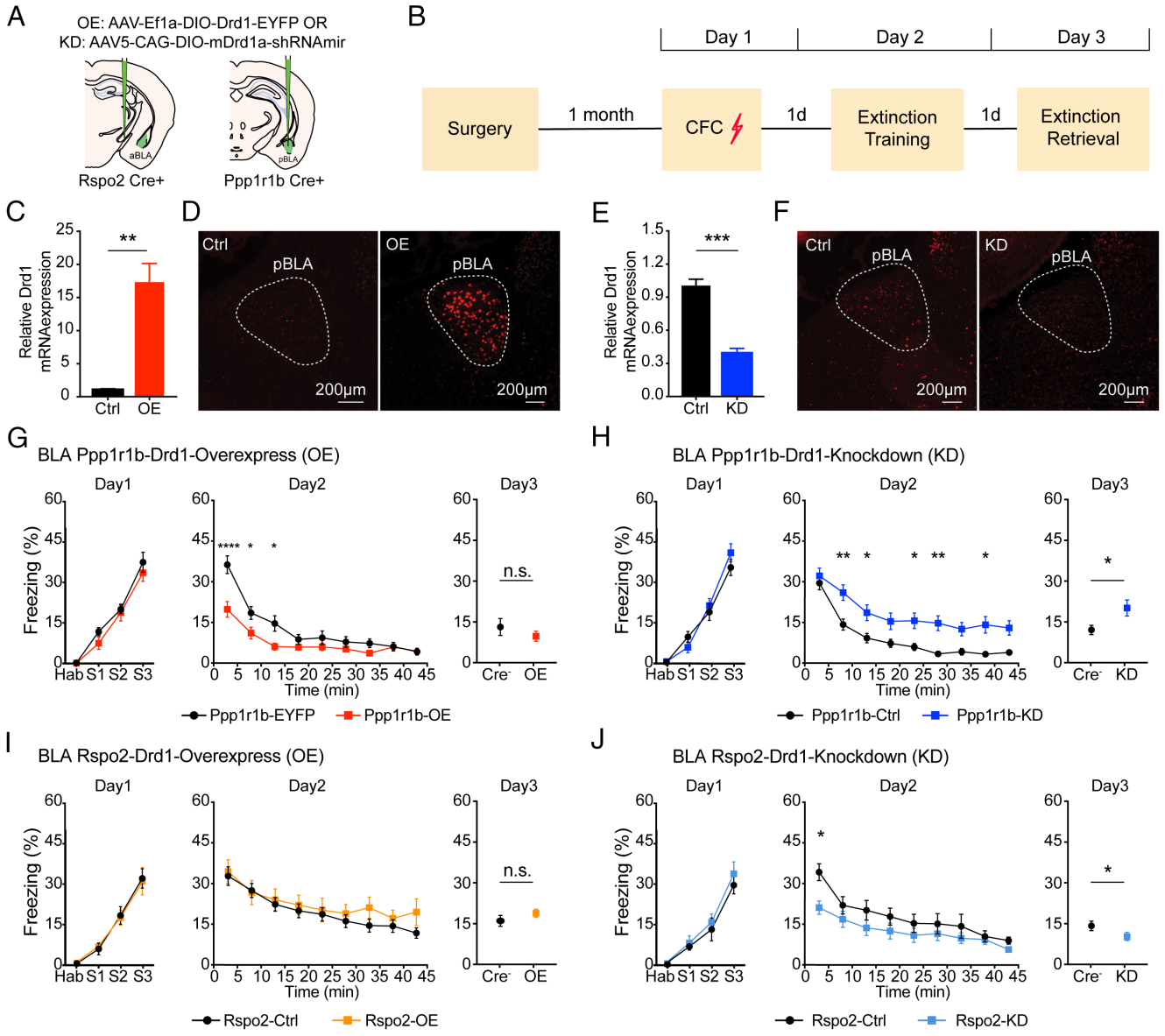

Fig. 5. Manipulation of Drd1 in *Rspo2* and *Ppp1r1b* neurons. (*A*) Schematic of the experimental procedure. An AAV-Ef1a-DIO-Drd1-EYFP or an AAV5-CAG-DIO-mDrd1a-shRNAmir injected in the pBLA or aBLA of *Rspo2* pr *Ppp1r1b* Cre mice to induce Drd1 overexpression or KD respectively. (*B*) Conditioning protocol. (*C*) Drd1 mRNA expression in pBLA for control (Ctrl) and overexpressing (OE) conditions. Unpaired *t* test, ***$P < 0.001$, **$P < 0.01$. (*D*) Confocal images showing D1 receptor overexpression in pBLA. (*E*) Drd1 mRNA expression in pBLA for Ctrl and KD conditions. Unpaired *t* test, ***$P < 0.001$, **$P < 0.01$. (*F*) Confocal images showing D1 receptor KD in pBLA. (*G*) Drd1 overexpression (OE) in BLA *Ppp1r1b*+ neurons caused significantly lower freezing level on Day 2 and Day 3. (*H*) Drd1 KD impaired extinction learning (Day 2) and memory (Day 3). (*I*) Drd1 overexpression (OE) in BLA *Rspo2*+ neurons did not cause a change in freezing level on Day 2 and Day 3. (*J*) Drd1 KD in BLA *Rspo2*+ did not impaired extinction learning (Day 2) and memory (Day 3). Two-way ANOVA, *$P < 0.05$, **$P < 0.01$, ***$P < 0.001$, ****$P < 0.0001$. Data are presented as mean ± SEM.

mostly nonoverlapping. This topology of projections involved in reward, aversion, and salience aligns with known anatomical and functional divisions of VTA dopaminergic neurons (38–41). The medial VTA projects to other reward regions, including the nucleus accumbens, which is involved in reward processing and reward prediction errors, and is necessary for fear extinction (14, 40). During fear extinction, medial VTA dopaminergic neurons encode a reward prediction error signal while lateral VTA encodes salience. Interestingly, during fear conditioning, both the medial and lateral VTA are activated by foot shocks, which is consistent with our finding that dopaminergic activity increases in both BLA populations in response to shock (16). It is worth noting that while our anatomical tracing experiments suggest that VTA projections to BLA fear and fear extinction neurons are largely nonoverlapping, they do not exclude the possibility that a subpopulation of VTA dopaminergic neurons sends collaterals to both. In addition, individual neurons in both the VTA and BLA can encode multiple task and behavioral features, so the clustering of VTA-BLA projections is likely more complex than what we have described here (24, 42, 43). Furthermore, our cell type–specific anatomical approach could not rule out contributions from additional dopaminergic regions, and the functional role of VTA TH^- neurons projecting to BLA remains unaddressed. Future studies should delineate the role of specific VTA-BLA projections in mediating diverse behaviors and associations.

Nature of the Dopaminergic Signal in BLA. Input from midbrain dopaminergic neurons could modulate the activity of BLA *Rspo2*$^+$ neurons and *Ppp1r1b*$^+$ neurons in several ways. In the dorsal striatum and nucleus accumbens, glutamate is

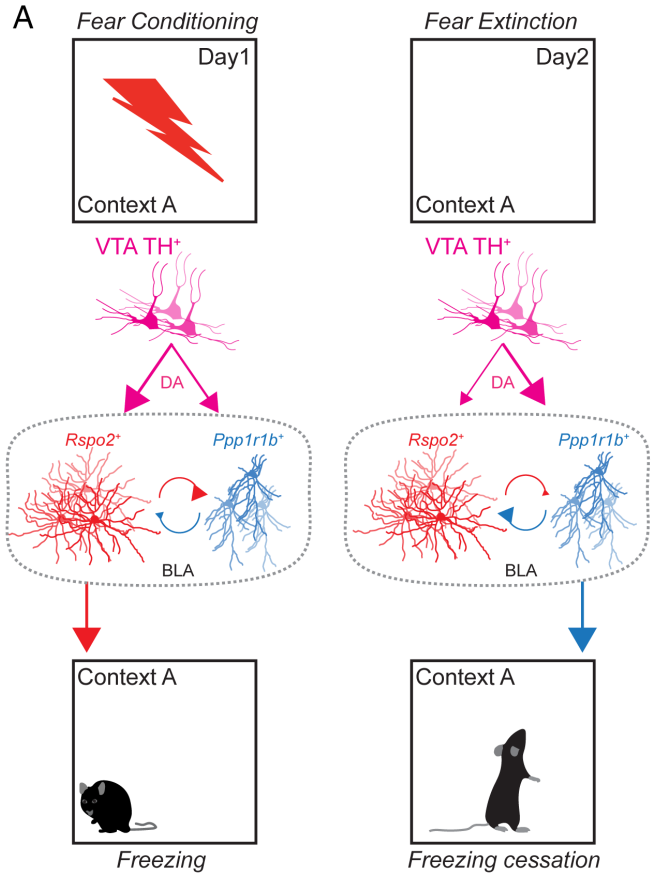

Fig. 6. Role of VTA DA innervation to *Rspo*$^+$ and *Ppp1r1b*$^+$ BLA neurons during fear conditioning and fear extinction. (*A*) Schematic model of the circuit activity in relation to fear conditioning and fear extinction. During fear conditioning (*Left*, *Top* to *Bottom*), the US (electric shock, red) causes DA release on both *Rspo2*$^+$ (red) and *Ppp1r1b*$^+$ (blue) BLA neurons engaged in a competitive inhibitory antagonism. The DA release is larger on *Rspo2*$^+$ BLA neurons, which in turn inhibit *Ppp1r1b*$^+$ BLA neurons promoting freezing. During fear extinction (*Right*, *Top* to *Bottom*), the lack of US causes DA release mainly on *Ppp1r1b*$^+$ BLA neurons, which in turn inhibit *Rspo2*$^+$ BLA neurons promoting freezing cessation.

coreleased with dopamine, which can directly increase firing rates (44–46). However, glutamate corelease has not been observed in the BLA, though see ref. 23. Based on our in situ results, the effect of dopamine on BLA neurons is mediated by D1 receptors, which enhance excitability through increases in cyclic adenosine monophosphate (cAMP) and activation of protein kinase A (30, 47, 48). The use of cell type–specific manipulations will be fundamental to dissect the role of dopamine in modulating additional amygdala subnuclei during extinction (46, 49).

Dopaminergic Modulation of Extinction Circuits. In addition to directly activating the *Ppp1r1b*$^+$fear extinction neurons in the BLA, VTA dopaminergic neurons indirectly contribute to fear extinction by stimulating neurons in other brain regions (36, 50). As a brain-wide neuromodulator, VTA dopaminergic neurons project to a distributed brain network, some of which likely contribute to the regulation of fear extinction learning and memory. These brain regions include the pBLA, the nucleus accumbens (Nac), and the medial prefrontal cortex (mPFC) (51–53). These brain regions receive inputs from distinct subsets of VTA dopaminergic neurons, where axonal terminals have been shown to report task-specific responses (8, 54). This connectivity pattern may reveal a projection-specific regulation of fear extinction operated by VTA dopaminergic neurons.

Inputs to the BLA and its outputs to the central amygdala are mediated by the intercalated cells (ITCs) (49, 55, 56). A recent evidence suggests that the two medial clusters of ITCs have opposing roles in behavior: Dorsomedial ITCs (dmITCs) promote fear expression and inhibit BLA fear extinction neurons, whereas ventromedial ITCs (vmITCs) promote fear suppression by inhibiting CeAs fear-producing neurons (49). During fear extinction, midbrain dopaminergic neurons can inhibit dmITCs causing the disinhibition of BLA extinction neurons and vmITCs (46, 49). Therefore, dopamine can modulate fear extinction behavior by disinhibiting the BLA *Ppp1r1b*$^+$-ITC-CeA disynaptic projection (57). The nucleus accumbens (Nac) is another downstream target of the BLA and VTA that is critical for appetitive behavior (8, 26, 58–60). Moreover, dopaminergic activity in the NAc is required for fear extinction learning (61, 62). During reward learning, the projection from the BLA to the NAc drives reward-seeking and is necessary for dopaminergic enhancement of NAc cue response (63, 64). Dopaminergic reward prediction error signals in the NAc are also necessary for fear extinction (14, 61). Therefore, fear extinction may also be modulated by the convergence of inputs from the BLA *Ppp1r1b*$^+$ neurons carrying CS information and VTA dopaminergic in the nucleus accumbens. Our findings of dopaminergic signaling in BLA *Ppp1r1b*$^+$ extinction neurons suggest that dopamine initiates fear extinction learning in the *Ppp1r1b*$^+$ neurons by modulation of local circuits and enhances downstream signaling to support fear extinction memory in a brain-wide circuit.

A Role for Dopamine in Fear Relapse. Fear extinction memory is notoriously unstable and learned fear often relapses to re-exposure to the US (fear reinstatement) or after the passage of time (spontaneous recovery). Prevention of fear relapse is a barrier to successful treatment of PTSD and other anxiety-related disorders (65). We showed a surprising effect that increasing dopaminergic activity at BLA fear neurons can rapidly reverse fear extinction and induce fear relapse (Fig. 4 *G* and *H*), even without re-exposure to the US (shock). This effect appeared during late extinction (Fig. 4 *G* and *H*), suggesting that increased dopaminergic activity in *Rspo2*$^+$ neurons does not affect fear memory recall or initial fear extinction learning. In contrast, direct activation of *Rspo2*$^+$ neurons impairs both fear extinction learning and memory (4). The neural circuit mechanisms underlying fear relapse are poorly understood, however, it may engage overlapping circuitry with fear conditioning. During fear reinstatement, VTA dopaminergic neurons also mediate inhibition of the infralimbic (IL) cortex (66). Together with our current results, this suggests that dopamine-dependent inactivation of IL and reactivation of BLA fear neurons could underlie fear relapse. These results add to a growing body of evidence of the role of dopamine in aversion (67). Additional experiments will be necessary to confirm this proposed circuit and its activity during fear reinstatement.

In conclusion, this study reveals a dopaminergic mechanism for fear extinction learning. VTA dopaminergic activity generated by the absence of expected aversive stimuli functions as a teaching signal to drive the amygdala extinction neurons for fear extinction learning.

Materials and Methods

Subjects. 8 to 16-wk-old male mice were used for all experiments. All Cre transgenic mice were bred using heterozygous males with females of C57BL/6 background. BLA Rspo2$^+$ neurons were targeted using Rspo2-Cre mice. BLA *Ppp1r1b*$^+$ neurons were targeted using Cartpt-Cre mice, which were previously validated for

genetic specificity. VTA dopaminergic neurons were targeted using DAT-IRES-Cre mice (Jackson Laboratory stock number: 006660). Mice undergoing all behavioral tests were singly housed for 1+ wk prior to experiments and kept on a 12 h light, 12 h dark–light cycle. Control mice for behavioral experiments underwent identical procedures as experimental mice but were Cre- mice of the same sex from the same litters. Wild-type mice used for in situ experiments were of the C57BL/6 background and were group-housed. All mice were maintained and cared for in accordance with protocols approved by the Massachusetts Institute of Technology (MIT) Committee on Animal Care (CAC) and guidelines by the NIH.

General Virus Surgery. For all subjects, surgeries were performed under aseptic conditions and body temperature was maintained with a hand warmer wrapped in Kimtech wipes. Rodents were anesthetized with ketamine and provided with 0.1 mg/kg slow-release Buprenex for analgesia. Subjects were then placed in a digital small animal stereotax. Following anesthesia, hair was removed from the dorsal scalp with hair clippers, ophthalmic ointment was applied to the eyes, the incision area was scrubbed three times with alcohol and betadine swabs, and 2% lidocaine was injected under the skin surface to provide local\anesthesia. Viral injections were performed using a mineral oil-filled glass micropipette attached to a 1 μL microsyringe delivering virus at a rate of 0.05 to 0.01 μL/min using a microsyringe pump and controller. After viral injection, 5 min were allowed to pass before the needle was slowly withdrawn. After infusions were complete, the incision was closed with nylon sutures. Subjects received a subcutaneous injection of 1 mL of warm Ringer's solutions and were maintained in a clean home cage placed on a heating pad at 35 °C until fully recovered from anesthesia. All measurements are made relative to bregma for virus and implant surgeries. For all experiments involving viral or tracer injections, animals containing mistargeted injections(s) were excluded after histological verification. Sample sizes were based on reports in related literature and were not predetermined by calculation.

Viral Constructs. We constructed a Cre-dependent AAV (AAV5-DIO-DA2m) carrying the second-generation $GRAB_{DA2m}$, abbreviated DA2m, which binds DA with medium affinity (35). AAV5-Ef1a-DIO-ChR2-EYFP (AV5226B) and AAV5-Ef1a-DIO-eYFP (AV4310D) were obtained from the University of North Carolina at Chapel Hill Vector Core. AAV5-Ef1a-DIO-eNpHR3.0-EYFP (Plasmid #26966) were obtained from Addgene. AAV1-synP-FLEXsTpEpB and RV-mCherry virus were obtained from Ian Wickersham laboratory at MIT. Constructs of AAV5-Ef1a-DIO-Drd1-EYFP and AAV5-CAG-DIO-GFP-mDRD1a-shRNAmir were generated in house and virus were acquired from the Gene Therapy Center and Vector Core at the University of Massachusetts Medical School. Virus plasmids are available through a material transfer agreement.

Anterograde tracing surgery. For anterograde tracing, 200 nL of AAV5-DIO-ChR2-EYFP was injected into the VTA of DAT-IRES-Cre mice (AP −3.2, ML +0.5, DV −4.5) and incubated for 4 wk.

Retrograde rabies tracing surgery. For monosynaptic retrograde rabies experiments, 150 nL of rabies helper virus, AAV1-synPFLEX-sTpEpB, was injected into the aBLA of Rpso2-Cre mice or pBLA of Ppp1r1b-Cre mice. Two weeks later, 150 nL EnvA G protein deleted rabies virus SADΔG-mCherry, was injected into the same location. 1 wk later, mice were killed and brain sections of VTA underwent IHC using antibodies against TH (Tyrosine Hydroxylase) and visualized using Alexa Fluor 647-conjugated secondary antibody (Invitrogen, Cat#A21244).

Optogenetic surgery. For terminal manipulation experiments, 200 μL of AAV5 Cre-dependent virus was bilaterally injected into the VTA of DAT-IRES-Cre mice (AP −3.10 mm, ML ±0.50 mm, DV −4.40 mm) and incubated for 3 to 4 wk before behavioral experiments. For optical implant surgery, two optic fibers (200 μm core diameter, 5.5 mm length; Doric Lenses) were bilaterally lowered above the injection sites (aBLA: −1.4 mm AP, ±3.4 mm ML, −4.7 mm DV; pBLA: −2.0 mm AP, ±3.4 mm ML, −4.7 mm DV). The implants were secured to the skull with two jewelry screws and adhesive cement (C&B Metabond). A protective cap, made using a 1.5 mL black Eppendorf tube, was fixed onto the implant using dental cement.

Fiber photometry surgery. For fiber photometry experiments, 200 μL of AAV5 Cre-dependent virus was unilaterally injected into the right aBLA of Rspo2-Cre mice (AP −1.4 mm, ML ±3.4 mm, DV −5.0 mm), and the pBLA of Ppp1r1b-Cre mice (AP −2.0 mm, ML ±3.4 mm, DV −4.9 mm) and incubated for 4 to 5 wk before behavioral experiments. For fiber implants, an optic fiber (400um core diameter, 5.5 mm length, screw fitting; Doric Lenses) was slowly lowered above the injection sites (aBLA: −1.4 mm AP, ±3.4 mm ML, −4.95 mm DV; pBLA: −2.1 mm AP, ±3.4 mm ML, −4.85 mm DV). The implant was secured to the skull with adhesive cement (C&B Metabond). A protective cap, custom designed to screw onto the implant, was used to prevent debris from damaging the optic fiber.

Anterograde Tracing. Mice were killed and brains sectioned sagittally at 50 μm on a vibratome. Every 3rd section (every 150 μm) containing the BLA and VTA were collected for analysis. Sections containing the VTA underwent IHC using antibodies against TH and visualized using Alexa Fluor 555-conjugated secondary antibody. Whole section images were collected at 10× magnification using a confocal microscope. Sections were registered to the brain atlas using Neuroinfo (MBF) and analyzed using ImageJ software. Images were background subtracted, and mean pixel intensity was measured.

In Situ Hybridization. For the examination of dopamine receptor coexpression with *Rspo2* and *Ppp1r1b* in the BLA, fresh frozen tissue samples were prepared for RNA-scope by ACDbio. Mice were deeply anesthetized with isoflurane and decapitated. Brains were extracted, and the cerebellum was removed to provide a flat surface. These brain sections were placed cut side down in a mold and covered with OCT, then flash-frozen in powdered dry ice. Molds remained in dry ice for 5 min before being wrapped in aluminum foil and placed in a plastic bag. Embedded tissue was stored at −80 degrees until sectioning. Prior to sectioning, brains were equilibrated to the cryostat temperature for 30 min. Brains were sectioned at 20um in a cryostat (chamber at 20 degrees, plate at 16 degrees) and thaw-mounted onto Colorfrost Plus slides (25 × 75 mm, Fisherbrand). Sections from three brains were serially thaw-mounted onto 20 slides through the BLA, anterior–posterior distance from Bregma (−0.8 mm to −2.4 mm). Slides were air-dried at room temperature for 60 min prior to storage at −80 degrees. smFISH for all genes examined–*Drd1*, *Drd2*, *Drd3, Drd4, DrD5, Ppp1r1b, Rspo2* was performed using RNAscope Fluorescent Multiplex Kit by Advanced Cell Diagnostics as described in their user manual. Slides were imaged by using confocal microscopy (Zeiss LSM 880) and fluorescence intensity was measured by using ImageJ software, upon background subtraction.

Cell Counting. Images of immunohistochemistry counting were acquired using confocal microscopy (Zeiss LSM700) under a 10× objective. Maximum intensity projections were generated using ZEN Blue software (Zeiss). Neurons stained against GFP (green), c-Fos (red), mCherry (Fos), and DAPI (blue) were automatically using cell counting software (ImageJ) with manual adjustment of detection thresholds. The region of interest (ROI) was defined manually based on anatomical landmarks. All counting was performed blind as to the group and condition that the specimen belonged to.

Contextual Fear Extinction Behavioral Protocol. The behavioral context were 29 × 25 × 22 cm chambers (Med Associates) with grid floors, opaque ceilings, white lighting, and scented with 5% benzaldehyde. Before fear conditioning, mice were habituated to investigator handling for 5 min on three consecutive days in the holding room where the mice were housed. For mice undergoing photometric recordings, mice were additionally attached and habituated to the recording cord for 2 d in their home cage for 20 min. On day 1 of CFE, mice were habituated in the behavioral context for 3 min, followed by three footshocks (0.60 mA, 2 s) delivered at 180 s, 250 s, and 320 s. Mice remained in the behavior chamber for 80 s after the third footshock and then returned to their home cages in the holding room. Overall, the training protocol lasted 400 s, a time sufficient to form a strong conditioning to the context. 24 h after fear conditioning, mice returned to the fear conditioning chambers to receive 45 min extinction training without any footshocks. Then mice were put back in their home cages for another 24 h. On Day 3, mice were placed in the conditioned context for 10 min extinction retrieval test. Behavior videos were recorded with VideoFreeze software and freezing level was scored manually by experimenters who were blinded to conditions or automatically with DeepLabCut behavior analysis toolbox and custom Python code (68). Analysis of freezing bouts: i) CFC training protocol: Freezing was scored during the first 180 s to get a baseline and every 70 s including shocks; ii) extinction protocol: Freezing was scored by counting bouts in 5 min bins for a total time of 45 min; iii) extinction recall: Freezing was scored during the first 3 min exclusively (nevertheless, we subject mice to a 10 min extinction recall protocol to collect a larger amount of data with fiber photometry).

Optogenetic Manipulation. To apply optogenetic activation/inhibition of dopaminergic axonal terminals in BLA during fear extinction training, mice were returned to the conditioned behavior chamber to receive 45 min fear extinction training. After the first 5 min, the mice received 8 cycles of 3 min optogenetic activation (450 to 470 nm, 8 to 12 mW, 20 Hz) or 3 min optical inhibition (520 to 550 nm, 8 to 12 mW, constant) with 2 min intervals. The analysis of extinction learning (lasting 45 min) was organized in 9 bins of 5 min each in such a way that beginning of each 5 min bin was subject to optogenetic manipulation, except for the first bin.

Fiber Photometry.

Recording setup. We used a 1-site fiber photometry system from Doric to collect DA2m signal. Prior to recording, mice were habituated to handling and attachment to the photometry cable. A 465 nm LED (to measure dopamine-dependent fluorescence changes reflecting dopamine levels) and 405 nm LED (to measure dopamine-independent change and serve as an internal control) were sinusoidally modulated at 211 HZ and 531 Hz, respectively, and passed through an integrated fluorescence minicube where beam splitters combine the excitation wavelengths and separate the emission wavelength (Fluorescence MiniCube FMC5, Doric Lenses). Excitation light was passed from the minicube through a 400 nm mono-fiber-optic patch cord to a rotary joint and through a dual fiber-optic low autofluorescence 400 nm NA 0.48 patch cord coupled to a 400 nm fiber optic implant positioned over the BLA. Emission fluorescence was collected through the same optic fibers and patch cords and separated in the fluorescence minicube and focused onto a femtowatt photoreceiver. Output control and the acquisition of input data was synchronized with a Doric Fiber Photometry console and Neuroscience Studio software.

Analysis. Raw photometry traces were preprocessed with custom Python scripts for timestamp corrections and alignment to behavior, then processed using the open-source photometry analysis tool, GuPPy. GuPPy was developed by the Lerner Lab at Northwestern. For CFC recordings, additional preprocessing was necessary. Due to the short length and prolonged shock responses, the linear regression used in the GuPPy software to fit the control signal to the signal produces poor results. We used the airPLS algorithm to subtract the background before processing with GuPPy as with the other recordings (69). Subjects that did not display an increase in dopamine activity to at least one of the stimuli, were excluded from analysis.

Statistical Analysis. GraphPad Prism (version 8.0 for Mac OS X, GraphPad Software, La Jolla, CA) and Python were used for statistical analysis. All data are presented as mean ± SEM. n indicates number of animals or number of cells. Box plots represent the median and 25th and 75th percentiles, and their whiskers represent the data range. Comparisons between two-group data were analyzed by the two-tailed unpaired *t* test or two-tailed paired *t* test. Multiple group comparisons were assessed using a One-way ANOVA or Two-way RM (Repeated Measures) ANOVA, followed by the Tukey's multiple comparison test when significant main effects or interactions were detected. The null hypothesis was rejected at the $P < 0.05$ level. Data met assumptions of statistical tests. See *SI Appendix*, Table S1 for statistics. Sample sizes were chosen on the basis of previous studies (4, 57).

Data, Materials, and Software Availability. All study data are included in the article and/or *SI Appendix*.

ACKNOWLEDGMENTS. This work was supported by the RIKEN Center for Brain Science, the HHMI, and the Freedom Together Foundation (S.T.). We thank J. Martin, X. Zhou, W. Yu, C. Lovett, A. Hamalian, and S. Y. Huang for technical assistance with experiments. We sincerely thank Dr. Ian Wickersham for providing the rabies virus and for guidance. We would like to thank Wickersham Lab Technical Associate, Heather Sullivan for providing support with viruses. We thank the generosity of Dr. Yulong Li of Peking University for providing the genetically encodable fluorescent dopamine indicator plasmid used to construct the virus. Portions of this text first appeared in the PhD thesis of coauthor K.F.

1. A. Shalev, I. Liberzon, C. Marmar, Post-traumatic stress disorder. *N. Engl. J. Med.* **376**, 2459–2469 (2017).
2. E. I. Martin, K. J. Ressler, E. Binder, C. B. Nemeroff, The neurobiology of anxiety disorders: Brain imaging, genetics, and psychoneuroendocrinology. *Psychiatr. Clin. North Am.* **32**, 549–575 (2009).
3. I. P. Pavlov, *Conditioned Reflexes* (Oxford University Press, 1927).
4. X. Zhang, J. Kim, S. Tonegawa, Amygdala reward neurons form and store fear extinction memory. *Neuron* **105**, 1077–1093.e7 (2020).
5. B. F. Grewe *et al.*, Neural ensemble dynamics underlying a long-term associative memory. *Nature* **543**, 670–675 (2017).
6. C. Herry *et al.*, Switching on and off fear by distinct neuronal circuits. *Nature* **454**, 600–606 (2008).
7. M. Pignatelli, A. Beyeler, Valence coding in amygdala circuits. *Curr. Opin. Behav. Sci.* **26**, 97–106 (2019).
8. J. Kim, M. Pignatelli, S. Xu, S. Itohara, S. Tonegawa, Antagonistic negative and positive neurons of the basolateral amygdala. *Nat. Neurosci.* **19**, 1636–1646 (2016).
9. W. Schultz, Dopamine reward prediction error coding. *Dialogues Clin. Neurosci.* **18**, 23–32 (2016).
10. S. B. McHugh *et al.*, Aversive prediction error signals in the amygdala. *J. Neurosci.* **34**, 9024–9033 (2014).
11. G. P. McNally, J. P. Johansen, H. T. Blair, Placing prediction into the fear circuit. *Trends Neurosci.* **34**, 283–292 (2011).
12. M. Watabe-Uchida, N. Eshel, N. Uchida, Neural circuitry of reward prediction error. *Annu. Rev. Neurosci.* **40**, 373–394 (2017).
13. W. Schultz, Reward prediction error. *Curr. Biol.* **27**, R369–R371 (2017).
14. R. Luo *et al.*, A dopaminergic switch for fear to safety transitions. *Nat. Commun.* **9**, 2483 (2018).
15. X. I. Salinas-Hernández *et al.*, Dopamine neurons drive fear extinction learning by signaling the omission of expected aversive outcomes. *Elife* **7**, e38818 (2018).
16. L. X. Cai *et al.*, Distinct signals in medial and lateral VTA dopamine neurons modulate fear extinction at different times. *Elife* **9**, e54936 (2020).
17. W. Tang, O. Kochubey, M. Kintscher, R. Schneggenburger, A VTA to basal amygdala dopamine projection contributes to signal salient somatosensory events during fear learning. *J. Neurosci.* **40**, 3969–3980 (2020).
18. A. R. de Oliveira *et al.*, Conditioned fear is modulated by D2 receptor pathway connecting the ventral tegmental area and basolateral amygdala. *Neurobiol. Learn. Mem.* **95**, 37–45 (2011).
19. K. Hori, J. Tanaka, M. Nomura, Effects of discrimination learning on the rat amygdala dopamine release: A microdialysis study. *Brain Res.* **621**, 296–300 (1993).
20. F. M. Inglis, B. Moghaddam, Dopaminergic innervation of the amygdala is highly responsive to stress. *J. Neurochem.* **72**, 1088–1094 (1999).
21. J. J. Walsh, M. H. Han, The heterogeneity of ventral tegmental area neurons: Projection functions in a mood-related context. *Neuroscience* **282**, 101–108 (2014).
22. B. A. Silva *et al.*, A thalamo-amygdalar circuit underlying the extinction of remote fear memories. *Nat. Neurosci.* **24**, 964–974 (2021).
23. A. Lutas *et al.*, State-specific gating of salient cues by midbrain dopaminergic input to basal amygdala. *Nat. Neurosci.* **22**, 1820–1833 (2019).
24. J. Roeper, Dissecting the diversity of midbrain dopamine neurons. *Trends Neurosci.* **36**, 336–342 (2013).
25. L. A. Gunaydin *et al.*, Natural neural projection dynamics underlying social behavior. *Cell* **157**, 1535–1551 (2014).
26. S. Lammel *et al.*, Input-specific control of reward and aversion in the ventral tegmental area. *Nature* **491**, 212–217 (2012).
27. T. K. Lavin, L. Jin, I. R. Wickersham, Monosynaptic tracing: A step-by-step protocol. *J. Chem. Neuroanat.* **102**, 101661 (2019).
28. K. Kohara *et al.*, Cell type-specific genetic and optogenetic tools reveal hippocampal CA2 circuits. *Nat. Neurosci.* **17**, 269–279 (2014).
29. J.-M. Beaulieu, R. R. Gainetdinov, The physiology, signaling, and pharmacology of dopamine receptors. *Pharmacol. Rev.* **63**, 182–217 (2011).
30. R. J. Scibilia, J. E. Lachowicz, C. D. Kilts, Topographic nonoverlapping distribution of D1 and D2 dopamine receptors in the amygdaloid nuclear complex of the rat brain. *Synapse* **11**, 146–154 (1992).
31. K. Fuxe *et al.*, The dopamine D1 receptor-rich main and paracapsular intercalated nerve cell groups of the rat amygdala: Relationship to the dopamine innervation. *Neuroscience* **119**, 733–746 (2003).
32. N. C. Huff, J. W. Rudy, The amygdala modulates hippocampus-dependent context memory formation and stores cue-shock associations. *Behav. Neurosci.* **118**, 53–62 (2004).
33. L. Calandreau, A. Desmedt, L. Decorte, R. Jaffard, A different recruitment of the lateral and basolateral amygdala promotes contextual or elemental conditioned association in Pavlovian fear conditioning. *Learn. Mem.* **12**, 383–388 (2005).
34. K. A. Goosens, S. Maren, Contextual and auditory fear conditioning are mediated by the lateral, basal, and central amygdaloid nuclei in rats. *Learn. Mem.* **8**, 148–155 (2001).
35. F. Sun *et al.*, A genetically encoded fluorescent sensor enables rapid and specific detection of dopamine in flies, fish, and mice. *Cell* **174**, 481–496.e19 (2018).
36. X. I. Salinas-Hernández, S. Duvarci, Dopamine in fear extinction. *Front. Synaptic Neurosci.* **13**, 635879 (2021).
37. R. Kalisch, A. M. V. Gerlicher, S. Duvarci, A dopaminergic basis for fear extinction. *Trends Cogn. Sci.* **23**, 274–277 (2019).
38. W. Menegas, B. M. Babayan, N. Uchida, M. Watabe-Uchida, Opposite initialization to novel cues in dopamine signaling in ventral and posterior striatum in mice. *Elife* **6**, e21886 (2017).
39. E. S. Bromberg-Martin, M. Matsumoto, O. Hikosaka, Dopamine in motivational control: Rewarding, aversive, and alerting. *Neuron* **68**, 815–834 (2010).
40. S. Ikemoto, Dopamine reward circuitry: Two projection systems from the ventral midbrain to the nucleus accumbens–olfactory tubercle complex. *Brain Res. Rev.* **56**, 27–78 (2007).
41. M. Matsumoto, O. Hikosaka, Two types of dopamine neuron distinctly convey positive and negative motivational signals. *Nature* **459**, 837–841 (2009).
42. B. Engelhard *et al.*, Specialized coding of sensory, motor and cognitive variables in VTA dopamine neurons. *Nature* **570**, 509–513 (2019).
43. K. M. Gothard, Multidimensional processing in the amygdala. *Nat. Rev. Neurosci.* **21**, 565–575 (2020).
44. S. Mingote *et al.*, Functional connectome analysis of dopamine neuron glutamatergic connections in forebrain regions. *J. Neurosci.* **35**, 16259–16271 (2015).
45. A. J. Granger, M. L. Wallace, B. L. Sabatini, Multi-transmitter neurons in the mammalian central nervous system. *Curr. Opin. Neurobiol.* **45**, 85–91 (2017).
46. A. Aksoy-Aksel, A. Gall, A. Seewald, F. Ferraguti, I. Ehrlich, Midbrain dopaminergic inputs gate amygdala intercalated cell clusters by distinct and cooperative mechanisms in male mice. *Elife* **10**, e63708 (2021).

47. M. P. de la Mora, A. Gallegos-Cari, Y. Arizmendi-García, D. Marcellino, K. Fuxe, Role of dopamine receptor mechanisms in the amygdaloid modulation of fear and anxiety: Structural and functional analysis. *Prog. Neurobiol.* **90**, 198–216 (2010).
48. J. A. Rosenkranz, A. A. Grace, Modulation of basolateral amygdala neuronal firing and afferent drive by dopamine receptor activation in vivo. *J. Neurosci.* **19**, 11027–11039 (1999).
49. K. M. Hagihara *et al.*, Intercalated amygdala clusters orchestrate a switch in fear state. *Nature* **594**, 403–407 (2021).
50. A. D. Abraham, K. A. Neve, K. M. Lattal, Dopamine and extinction: A convergence of theory with fear and reward circuitry. *Neurobiol. Learn. Mem.* **108**, 65–77 (2014).
51. P. W. Kalivas, P. Duffy, Time course of extracellular dopamine and behavioral sensitization to cocaine. I. Dopamine axon terminals. *J. Neurosci.* **13**, 266–275 (1993).
52. K. T. Beier *et al.*, Circuit architecture of VTA dopamine neurons revealed by systematic input-output mapping. *Cell* **162**, 622–634 (2015).
53. A. Björklund, S. B. Dunnett, Dopamine neuron systems in the brain: An update. *Trends Neurosci.* **30**, 194–202 (2007).
54. K. E. Parker *et al.*, A paranigral VTA nociceptin circuit that constrains motivation for reward. *Cell* **178**, 653–671.e19 (2019).
55. E. Likhtik, D. Popa, J. Apergis-Schoute, G. A. Fidacaro, D. Paré, Amygdala intercalated neurons are required for expression of fear extinction. *Nature* **454**, 642–645 (2008).
56. L. R. Johnson, J. E. Le Doux, "Amygdala microcircuits" in *Handbook of Brain Microcircuits*, G. Sheperd, S. Grillner, Eds. (Oxford University Press, ed. 2, 2018), pp. 185–198, New to this Edition.
57. J. Kim, X. Zhang, S. Muralidhar, S. A. LeBlanc, S. Tonegawa, Basolateral to central amygdala neural circuits for appetitive behaviors. *Neuron* **93**, 1464–1479.e5 (2017).
58. X. Zhang *et al.*, Genetically identified amygdala–striatal circuits for valence-specific behaviors. *Nat. Neurosci.* **24**, 1586–1600 (2021).
59. A. Beyeler *et al.*, Divergent routing of positive and negative information from the amygdala during memory retrieval. *Neuron* **90**, 348–361 (2016).
60. M. R. Stefani, B. Moghaddam, Rule learning and reward contingency are associated with dissociable patterns of dopamine activation in the rat prefrontal cortex, nucleus accumbens, and dorsal striatum. *J. Neurosci.* **26**, 8810–8818 (2006).
61. O. Holtzman-Assif, V. Laurent, R. F. Westbrook, Blockade of dopamine activity in the nucleus accumbens impairs learning extinction of conditioned fear. *Learn. Mem.* **17**, 71–75 (2010).
62. J. R. Bergado Acosta, E. Kahl, G. Kogias, T. C. Uzuneser, M. Fendt, Relief learning requires a coincident activation of dopamine D1 and NMDA receptors within the nucleus accumbens. *Neuropharmacology* **114**, 58–66 (2017).
63. G. D. Stuber *et al.*, Excitatory transmission from the amygdala to nucleus accumbens facilitates reward seeking. *Nature* **475**, 377–380 (2011).
64. F. Ambroggi, A. Ishikawa, H. L. Fields, S. M. Nicola, Basolateral amygdala neurons facilitate reward-seeking behavior by exciting nucleus accumbens neurons. *Neuron* **59**, 648–661 (2008).
65. K. M. Myers, M. Davis, Mechanisms of fear extinction. *Mol. Psychiatry* **12**, 120–150 (2007).
66. N. Hitora-Imamura *et al.*, Prefrontal dopamine regulates fear reinstatement through the downregulation of extinction circuits. *Elife* **4**, e08274 (2015).
67. J. P. H. Verharen, Y. Zhu, S. Lammel, Aversion hot spots in the dopamine system. *Curr. Opin. Neurobiol.* **64**, 46–52 (2020).
68. A. Mathis *et al.*, DeepLabCut: Markerless pose estimation of user-defined body parts with deep learning. *Nat. Neurosci.* **21**, 1281–1289 (2018).
69. E. Martianova, S. Aronson, C. D. Proulx, Multi-fiber photometry to record neural activity in freely-moving animals. *J. Vis. Exp.* **152**, e60278 (2019), 10.3791/60278.